Front. Energy 2023, 17(6): 811–821
https://doi.org/10.1007/s11708-022-0848-2

RESEARCH ARTICLE

Jinlong WANG, Jin XIAO, Yingdong CHENG, Zhen HUANG

Design and modeling of a free-piston engine generator

Abstract Free-piston engine generators (FPEGs) can be applied as decarbonized range extenders for electric vehicles because of their high thermal efficiency, low friction loss, and ultimate fuel flexibility. In this paper, a parameter-decoupling approach is proposed to model the design of an FPEG. The parameter-decoupling approach first divides the FPEG into three parts: a two-stroke engine, an integrated scavenging pump, and a linear permanent magnet synchronous machine (LPMSM). Then, each of these is designed according to predefined specifications and performance targets. Using this decoupling approach, a numerical model of the FPEG, including the three aforementioned parts, was developed. Empirical equations were adopted to design the engine and scavenging pump, while special considerations were applied for the LPMSM. A finite element model with a multi-objective genetic algorithm was adopted for its design. The finite element model results were fed back to the numerical model to update the LPMSM with increased fidelity. The designed FPEG produced 10.2 kW of electric power with an overall system efficiency of 38.5% in a stable manner. The model provides a solid foundation for the manufacturing of related FPEG prototypes.

Keywords free-piston engine generator, linear permanent magnet synchronous machine, system design, numerical model, finite element method

1 Introduction

1.1 Background

The transportation sector is currently one of the world's top contributors of greenhouse gas emissions [1,2]. As a result, both industry and academia are seeking ways to decarbonize the sector [3,4]. One promising technology is the free-piston engine generator (FPEG). Unlike the conventional range extender, which combines an internal combustion engine and electrical motor, the FPEG performs the same functions with a simplified structure. In the FPEG, the mechanical crankshaft is eliminated and electric power is produced by the linear piston motion with a high thermal and mechanical efficiency [5–7]. In addition, owing to the absence of a crankshaft, the FPEG can achieve various compression ratios and thus employ various renewable fuels to facilitate decarbonization [8].

1.2 Literature review

Various research methods and prototype designs have been proposed based on the FPEG concept. Shoukry et al. [9] of West Virginia University proposed a time-based model to investigate the performance of two-stroke direct-injection compression engines. A sinusoidal function was used to represent the alternator model based on a permanent magnet machine with a resistive load. The solution of combined dynamic and thermodynamic numerical equations enabled the detailed analyses of two-stroke direct-injection linear engine operations.

Researchers at Chalmers University of Technology [10] developed a dynamic model to predict the piston motion and frequency. BOOST and SENKIN were used to simulate the air exchange and combustion. The electric force of the alternator was applied to 90% of the strokes at a constant value, excluding the turning points when the piston speed was low. Various fuels were tested in the homogeneous charge compression ignition combustion mode.

Mikalsen and Roskilly [11–13] of Newcastle University presented a design of a modular compression ignition free-piston engine with a 44.4 kW output. Based on standard feedback ideas, they proposed a control strategy that provides adequate performance for moderate load changes.

Li et al. [14] of Shanghai Jiao Tong University used MATLAB/Simulink, Chemkin, and the finite element method (FEM) to investigate the performance of a newly developed two-stroke free-piston engine for electric

Received May 24, 2022; accepted Aug. 10, 2022; online Dec. 30, 2022

Jinlong WANG, Jin XIAO (✉), Yingdong CHENG, Zhen HUANG
Key Laboratory for Power Machinery and Engineering (Ministry of Education), Shanghai Jiao Tong University, Shanghai 200240, China
E-mail: xiaojin@sjtu.edu.cn

power generation. Through comparisons with the FEM model, they verified the effectiveness of the thrust-force waveforms predicted by an analytical model of the alternator. Resistance loads and equivalence ratios were also studied, and the results showed that the FPEG had a buildup trait that changed the top dead center (TDC) according to the load and other parameters.

Mao et al. [15] of the Beijing Institute of Technology proposed a parameter-coupling designation method for a diesel free-piston linear alternator. Computational fluid dynamics was used to calculate the progress of scavenging and combustion, the results of which were fed into the 0D numerical simulation. Their results showed that the free-piston engine alternator with optimal parameters operated with a good scavenging performance.

Jia et al. [16] developed a numerical model of a spark-ignited FPEG and validated the model with test results. Both the heat transfer and air leakage were considered. In the starting phase, the alternator thrust force remained constant. During stable operations, the load force was the product of the speed and load coefficient. Their results showed that the simulation data were in good agreement with the prototype test data.

Zhang et al. [17,18] of the University of Minnesota developed a numerical model of an opposed-piston, opposed-cylinder free-piston engine. The model was then utilized to develop a so-called “virtual crankshaft” that could regulate the piston motion by tracking a prescribed reference in real time.

In 2014, researchers [19,20] at Toyota Central R&D Laboratories Inc. adopted a W-shaped piston to develop a prototype FPEG with an electrical power of 10 kW. Numerical simulations and experiments were used to verify the motion control precision. The generator model parameters fit the actual characteristics without considering the magnetic saturation or iron loss. A second prototype linear permanent magnet synchronous machine (LPMSM) adopted a Halbach array of permanent magnets and rectangular wire, which achieved a higher voltage with a smaller current. Using the resonant pendulum-type control method, the distance between the TDC and bottom dead center (BDC) was controlled within 1 mm in both the motoring and firing modes [21,22].

Despite the studies on the modeling of FPEGs, most researchers tend to adopt simplified linear machine models to simulate the FPEG. Hence, the actual operation of the FPEG is not represented. Moreover, improper system design can lead to problems, such as misfiring or unstable operation. Therefore, it is necessary to integrate the actual electromagnetic force and proper system parameters into the FPEG model to obtain a better understanding of the FPEG.

1.3 Methodology

In this study, based on a previous project [23], a decoupling modeling design was applied to a single-piston FPEG (Fig. 1). The specifications were optimized to scale the output power of the system to 10 kW. Special attention was paid to the design of the scavenging pump to charge the air intake to 1.5 bar with a high scavenging efficiency. An FEM model was also developed to identify the optimal parameters of an LPMSM through a multi-objective genetic algorithm (MOGA). Unlike empirical

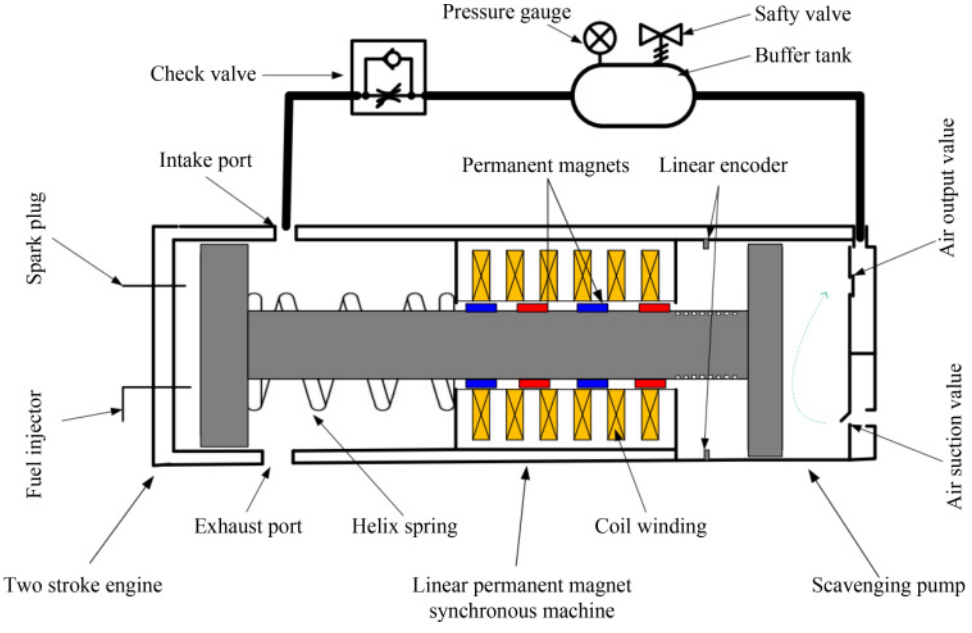

Fig. 1 Schematic diagram of FPEG.

models, the FEM model represents the LPMSM operation with increased fidelity and offers practical insights into the dynamic behavior of FPEGs [14].

2 Basic structure of FPEG system

Figure 1 shows a schematic of the FPEG system with three main components: a two-stroke gasoline engine, an LPMSM, and integrated scavenging pump. For the two-stroke gasoline engine, in-cylinder direct injection, spark plug ignition, and loop-scavenging structures were employed. The tubular type of LPMSM was selected in the FPEG, and permanent magnets were mounted on the translator. It is worth noting that the LPMSM can function as a linear electric motor in the starting phase and an electric generator in the combustion phase. The scavenging pump increases the air intake pressure and delivers a sufficient amount of fresh charge to the combustion chamber of the engine. The scavenging pump has two valves: an air suction valve and air output valve. When the piston moves from right to left and the air suction valve passively opens, fresh air enters the scavenging pump chamber owing to the pressure difference. In contrast, when the piston moves from left to right and the air output valve is open, fresh air is compressed and pumped into the combustion chamber of the engine. A helix spring is used as the rebound device in the FPEG, and a buffer tank maintains the scavenging pressure level during operations.

3 Parameter-decoupling design of the FPEG

3.1 Overall architecture

The overall architecture of the parameter-decoupling modeling design is shown in Fig. 2. The entire process is divided into six steps:

Step 1: Determine the overall FPEG target performance.

Step 2: Determine the engine and LPMSM output power based on the energy flow analysis.

Step 3: Design the engine and scavenging pump according to the required engine performance.

Step 4: Apply the results in Step 3 to develop a dynamic model of the FPEG in MATLAB/Simulink.

Step 5: Based on the simulation output in Step 4, develop an FEM model for the LPMSM and optimize its design through the MOGA.

Step 6: Feed the optimized FEM LPMSM parameters back into the dynamic model and finalize the FPEG design.

The detailed process of each step is described in the following Sections. The effectiveness of the final design is proven by the stable operation of the simulated FPEG system.

3.2 Target performance and energy flow analysis

The goal is to design a 10 kW FPEG with an overall efficiency above 35% [19,20,24–27]. The FPEG should also possess a maximum stroke of 90 mm and operate at a default frequency of 30 Hz. The required generator efficiency was set as 93% [21,28]. These performance targets will be adopted throughout the design process.

In general, chemical energy from the fuel is converted into electrical energy with combustion energy loss, heat transfer loss, mechanical energy loss, and joule loss. The fuel energy per cycle and fuel injection amount can be derived by the following equation:

$$Q_{\text{fuel}} = m_{\text{fuel}} H_u \eta_c = P_{\text{fuel}} \frac{1}{f} = \frac{P_e}{\eta_s} \frac{1}{f}, \tag{1}$$

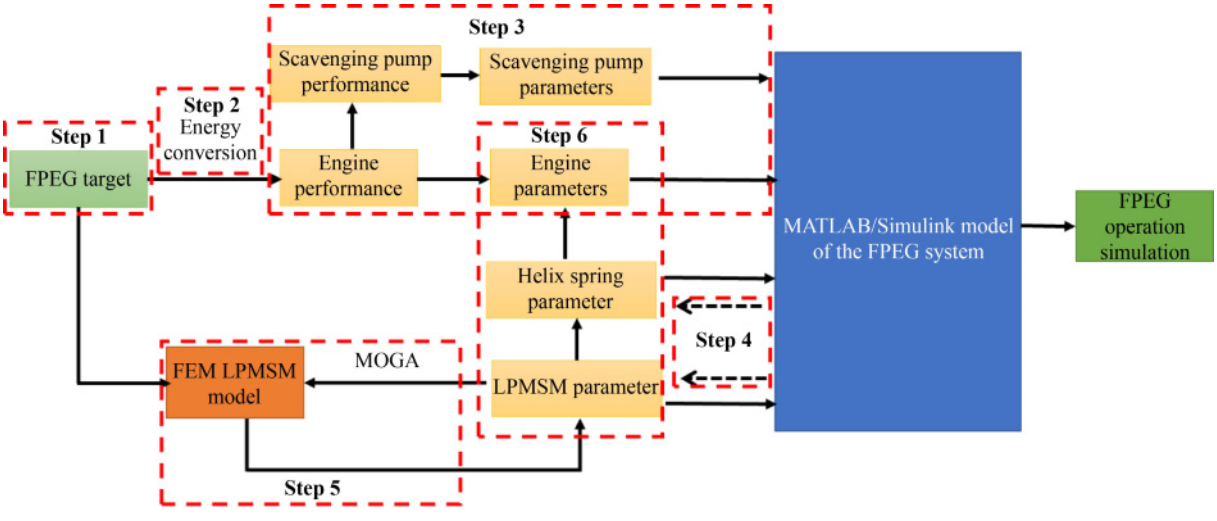

Fig. 2 Overall schematic of the parameter-decoupling design approach.

where Q_{fuel} is the energy from the fuel per cycle, P_e is the electrical power, η_s *is* the system efficiency, and f is the frequency of the FPEG operation (Hz). Assuming a combustion efficiency η_c = 97% and calorific value of fuel $H_u = 4.4 \times 10^7$ J/kg, the energy from fuel per cycle Q_{fuel} and desired fuel amount per cycle m_{fuel} were determined as 952.2 J and as 22.31 mg, respectively.

By setting the generator efficiency η_e = 93%, the desired engine output power can be calculated as

$$\eta_e = \frac{P_e}{P_{engine}}, \tag{2}$$

where P_{engine} is calculated as 10.75 kW. This parameter will be used for the engine design.

3.3 Design of engine and scavenging pump

Because the maximal stroke S was assumed to be 90 mm, the displacement volume and stroke-to-bore ratio were easily derived after the bore of the engine was determined, which should be set based on the target mean effective pressure. The process is as follows.

First, the equivalent engine speed is calculated by considering the number of strokes per cycle N_{stroke} and operational frequency f [24].

$$n_{crank} = 30 N_{stroke} f. \tag{3}$$

The mean effective pressure P_{mean} can be calculated by Eq. (4) [24].

$$P_{mean} = \frac{120 N_{stroke} P_{engine}}{\pi N_{cylinder} n_{crank} D^2 S}. \tag{4}$$

By substituting Eq. (3) into Eq. (4), and plugging all the values from the target performance in Section 3.2, the engine bore can be determined as

$$D = \sqrt{\frac{120 N_{stroke} P_{engine}}{\pi N_{cylinder} P_{mean} n_{crank} S}}. \tag{5}$$

For a conventional internal combustion engine, the mean effective pressure (MEP) often ranges between 0.78 MPa and 1.2 MPa [24]. Through Eq. (5), the engine bore within the MEP range can be derived, as shown in Fig. 3.

Figure 3 shows that when the stroke is constant, the stroke-to-bore ratio S/B increased with the increase in the MEP. Our previous project showed that the MEP of an FPEG could reach 1.04 MPa [23]. Here, the engine bore was designed as 70 mm with an S/B of 1.286 after rounding. Extensive studies have shown that FPEGs with a rated power of 10 kW have a compression ratio (CR) of approximately 10 [21,24–26]. Therefore, the CR was selected as 10. The main geometric parameters of the inlet and exhaust ports were determined according to Ref. [29].

After obtaining the two-stroke engine design, we now consider the design of the integrated scavenging pump.

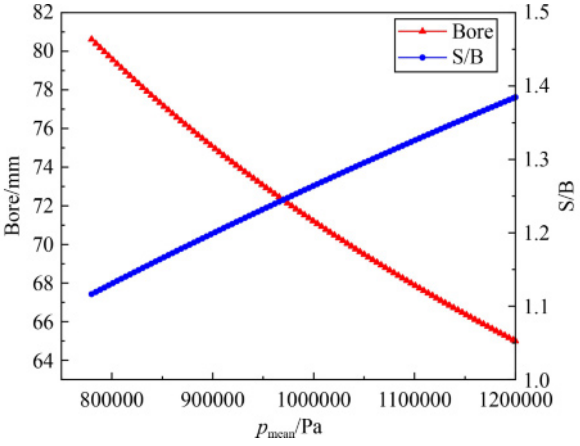

Fig. 3 Stroke-to-bore ratio and bore required for an engine.

Given the mass flow rate of air $\dot{m}_a$, the volumetric flow rate of air can be derived as [30]

$$\dot{V}_a = \frac{\dot{m}_a}{\rho_0}, \tag{6}$$

where $\dot{V}_a$ is the volumetric flow rate of air and ρ_0 is the air density.

It is widely known that air loss occurs in the scavenging pump owing to volumetric issues, pressure differences, and leakage. Thus, the correction volume should be calculated as [30]

$$V_c = \frac{\dot{V}_a}{\lambda_v \lambda_p \lambda_T \lambda_l}, \tag{7}$$

where λ_v, λ_p, λ_T, and λ_l are the volumetric, pressure, temperature, and leakage coefficients, respectively; and V_c is the final correction volume. The volumetric coefficient can be calculated as [31]

$$\lambda_v = 1 - a\left(\frac{\varepsilon_1}{\varepsilon_2} \cdot \left(\frac{p_2}{p_1}\right)^{1/(1+0.62(\gamma-1))} - 1\right), \tag{8}$$

where ε_1 and ε_2 are the compressibility coefficients of 0.99 and 0.98 under suction and discharge conditions, respectively. p_2 is the scavenged charged pressure of 1.5 bar based on Ref. [32], and the suction pressure p_1 was set as 1.0 bar [30]. Given the above information, the volumetric coefficient was calculated as 0.968. The authors further assumed that the pressure, temperature, and leakage coefficients are 0.97, 0.97, 0.935, respectively [30].

By combining Eqs. (6)–(8), the bore of the scavenging pump D_{sca} can be derived as

$$D_{sca} = \sqrt{\frac{4\dot{m}_a}{\pi S \lambda_v \lambda_p \lambda_T \lambda_l \rho_0}}. \tag{9}$$

The equivalence ratio δ can be determined as

$$\delta = \frac{\dot{m}_f}{F_s \dot{m}_a}. \tag{10}$$

The fuel injection amount per cycle $\dot{m}_f$ was set as 22.31 mg (see Section 3.2) and F_s is the stoichiometric fuel-air ratio.

Figure 4 shows the effects of different air masses on the required scavenging pump bore and corresponding equivalence ratio. It can be observed that an increase in the equivalence ratio reduced the scavenging pump bore. According to Ref. [29], to achieve a highly efficient scavenging process, the delivery ratio must reach 1.5. In this study, the delivery ratio was set as 2 by considering some design margins. To achieve this goal, δ must be set as 0.52, which indicates that the scavenging pump bore D_{sca} is approximately 90 mm after rounding.

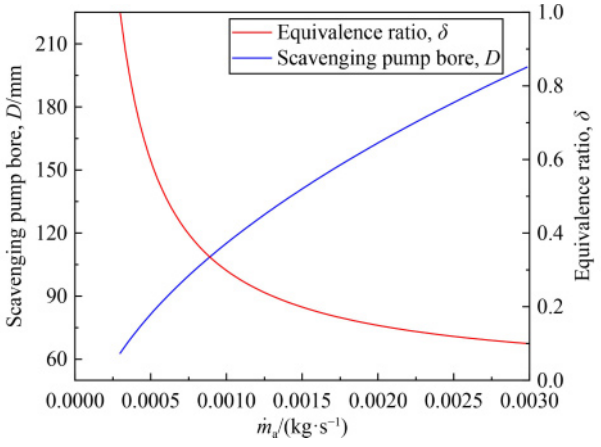

Fig. 4 Effects of varying the mass flow rate of air $\dot{m}_a$.

3.4 Dynamic model analysis

After obtaining the main parameters of the engine and scavenging pump, a dynamic model of the FPEG system was developed to validate their design. The dynamic model can also be applied to design other components, such as the helix spring and LPMSM. The dynamic model was developed in MATLAB/Simulink based on previous studies [9,10,14–16,18,33,34], as shown in Fig. 5. The electromagnetic force of the LPMSM can be derived as Eq. (11), which is proportional to the piston velocity when generating the load coefficient k_L [35]. Afterwards, the elasticity coefficient k of the helix spring and the generating load coefficient k_L of the LPMSM were calibrated to achieve stable operations of the simulated FPEG.

$$F_{mag} = k_L \dot{x}, \tag{11}$$

where x is the translator position.

Table 1 lists the parameter pairs considered, while Fig. 6 shows the corresponding simulation results. The simulation results show that the parameter pairs in Case 1 ensure the stable operation of the FPEG system with a 90 mm stroke and 30 Hz frequency. The other five cases were adjusted based on Case 1 to investigate the influence of various load coefficients k_L and elasticity coefficients k on the FPEG system operation.

• Case 2 could not achieve a stable performance because of the excess energy transferred to the LPMSM and the large load coefficient k_L.

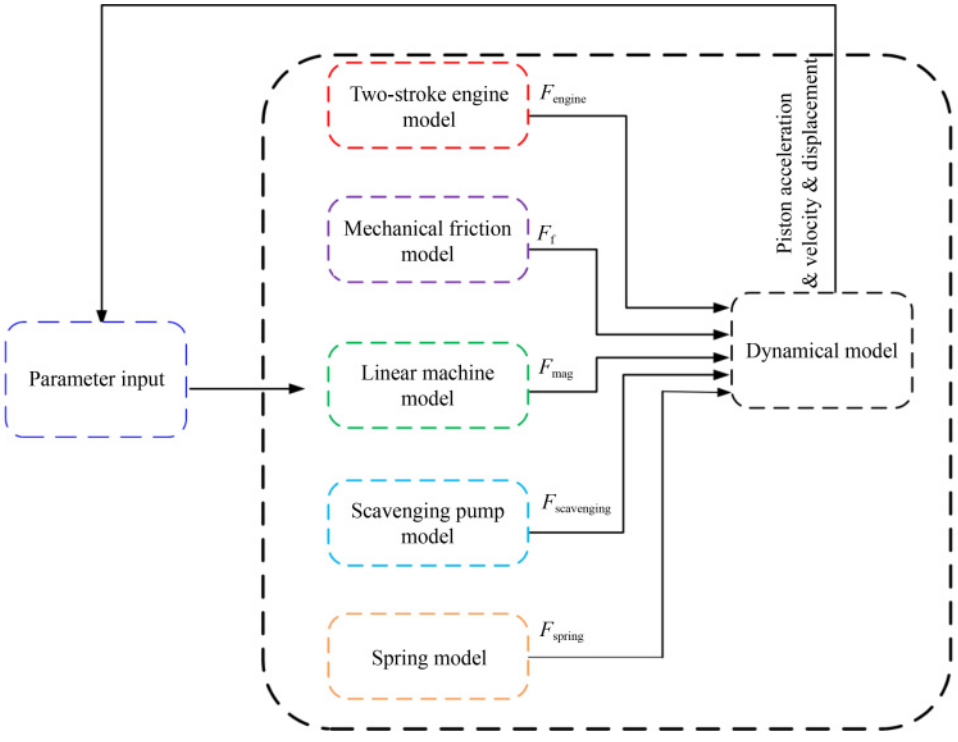

Fig. 5 Diagram of simulation model.

Table 1 Cases studies of the elasticity coefficient k and generating load coefficient k_L

Case number	Case 1	Case 2	Case 3	Case 4	Case 5	Case 6
$k/(10^4\ \mathrm{N\cdot m^{-1}})$	6.5	6.5	6.5	5	8	6.5
$k_L/(\mathrm{N\cdot(m/s)^{-1}})$	316	360	330	316	316	300

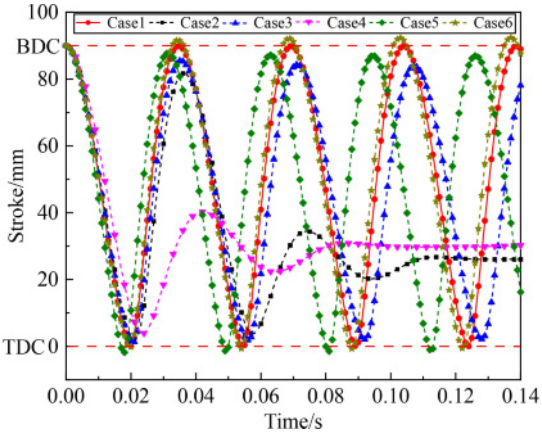

Fig. 6 Influence of stroke in different cases.

• Case 3 achieved the reciprocating performance with a smaller stroke.

• Case 4 failed because the spring could not provide sufficient energy to push the piston back properly.

• The piston in Case 5 exceeded the TDC point owing to the excessive spring energy.

• The piston in Case 6 exceeded the BDC point because the smaller generating load coefficient k_L led to the ineffective transfer of fuel energy to the LPMSM.

The parameter pair in Case 1 was selected as the initial parameters of the helix spring and LPMSM in the dynamic model. The piston speed profile and electrical output power of the LPMSM were simulated, as shown in Fig. 7. It is clear that the 10 kW output power was achieved at a piston speed of approximately 5.8 m/s. This speed was adopted to develop the FEM model of the LPMSM.

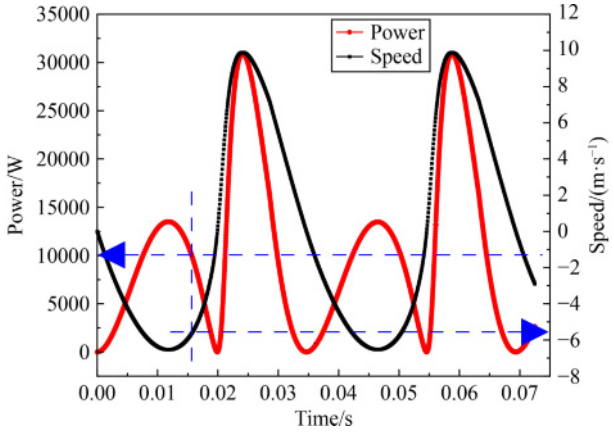

Fig. 7 The generated electric power and piston speed profile of the LPMSM in Case 1.

3.5 Design and analysis of the LPMSM through FEM

In this study, a tubular-type LPMSM was selected owing to its high compactness, reduced weight, and high efficiency [28,36]. Figure 8 shows the basic structure of the designed LPMSM, which mainly consists of a stator core and translator. The stator core has 42 slots and is made of a soft magnetic composite (Somaloy 500HR). The coils around the stator are made of copper. The translator consists of a yoke and quasi-Halbach-type ring-formed magnets. Figure 8(b) shows a cross-sectional view of this alternator, which indicates the structural parameters used for optimization.

3.5.1 Optimal design of the LPMSM through MOGA

The design optimization procedure includes four steps. First, the initial design of the LPMSM and the related 2D FEM model (Fig. 8(b)) were developed. The initial values of all the design parameters were calculated based on the theory in Ref. [36] (also shown in Table 2). Second, the optimization was formulated by selecting the design parameters and objective function. Table 2

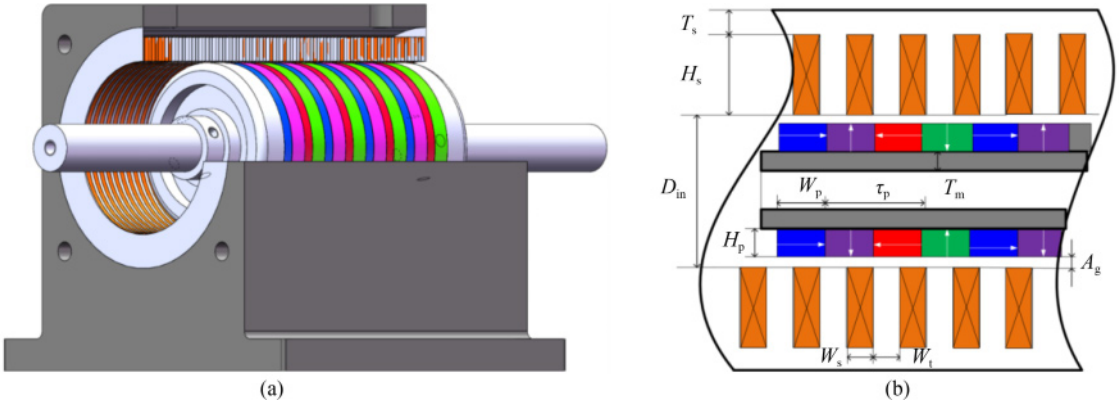

Fig. 8 The basic structure of the LPMSM. (a) 3D model; (b) 2D model.

summarizes the design parameters of the optimal design process. The objective function minimizes the cogging force while ensuring that the no-load phase voltage is within the designed range (as shown in Table 3). Third, the LPMSM model undergoes the optimal design process. A constant speed of 5.8 m/s based on the dynamic model results was selected as the preliminary speed profile of the translator. The MOGA was chosen to solve the optimization. After the optimal design parameters were determined, a 3D FEM model of the LPMSM was developed to facilitate the analysis of the alternator operation. In addition, a thermal analysis was conducted using the 3D FEM model to verify the rationality of the design.

Table 2 The geometrical dimensions and design variables of LPMSM

Item	Symbol	Value		
Number of slots	N_s	42		
Number of poles	N_p	8		
Pole pitch/mm	τ_p	18		
Turns per coil	N	32		
Air gap/mm	A_g	1		
Design variables	**Symbol**	**Initial**	**Range**	**Optimized**
Slot width/mm	W_s	3	[2.95,3.5]	3.44
Inner diameter/mm	D_{in}	60	[35,65]	55
Height slot/mm	H_s	12	[12,16]	15.15
Back iron height/mm	T_s	6	[4,10]	6.75
Axial PM width/mm	W_p	10	[5.4,12.6]	6.72
PM thickness/mm	H_p	5	[4.5,15]	5.54
Core thickness of mover/mm	T_m	10	[3,6]	5.43

Table 3 The objective function in MOGA

Cogging force RMS/N	No-load phase voltage RMS/V
Minimize	$330 < V < 340$

The initial and optimized values of the design variables are listed in Table 2. The final results converged after 26 generations, as shown in Fig. 9. With the optimal design, the maximum cogging force of the LPMSM was reduced from over 1000 to less than 55 N, as shown in Fig. 10.

3.5.2 Operation analysis at generating state

In general, the output power and efficiency of the FPEG are both determined by the external resistance load R. Figure 11 shows the output power and efficiency with various external resistance loads simulated from the FEM model. The output power first increased and then decreased. When the load is 8–34 Ω, the output power is over 10 kW, with a maximum power of 11.06 kW at 22 Ω. The generator efficiency increased as the load increased. When R = 33 Ω, the LPMSM produced 10.26 kW of electric power at 99.34% efficiency, which is comparable to that in Ref. [28].

Figure 12 shows the output power according to the speed profile in Fig. 7 when R = 33 Ω. It can be seen that in the high-speed section (right side of Fig. 12), the LPMSM produced a greater amount of electric power. The main reason for this is that the counter-electromotive force is proportional to both the flux linkage and piston speed, whereas the former has little variations in different phases. Therefore, speed has the greatest influence on electric power generation.

Through the FEM model, the relationship between the electromagnetic force and related piston speed was captured with increased fidelity, as shown in Fig. 13. The fitting equation, i.e., Eq. (12), was obtained, which represents the actual working process of the LPMSM. Therefore, Eq. (12) was fed back into the dynamic model to replace Eq. (11) and simulate the LPMSM generation state with increased fidelity.

$$F_{mag} = -12.25 + 443.09v - 2.397v^2 - 3.04v^3 + 0.056v^4 + 0.00658v^5. \quad (12)$$

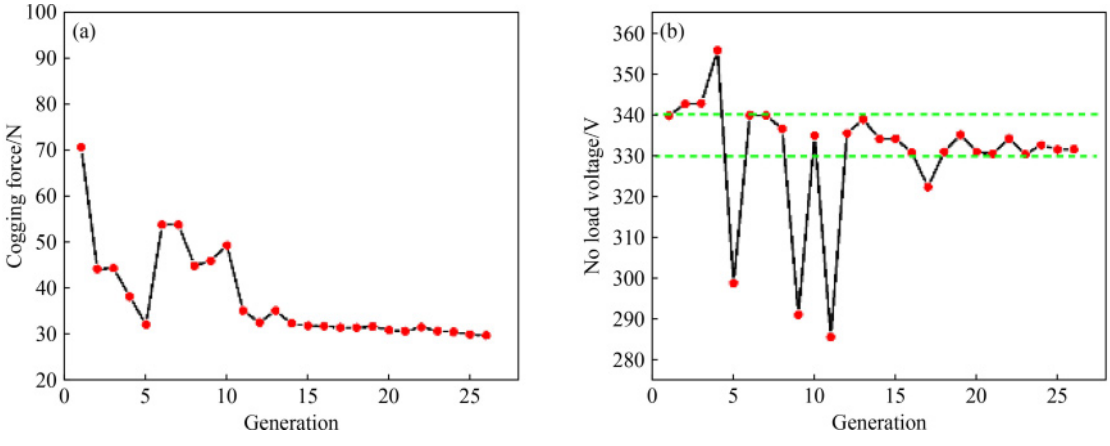

Fig. 9 Achieved the objectives results through MOGA optimization.
(a) Cogging force; (b) no-load phase voltage.

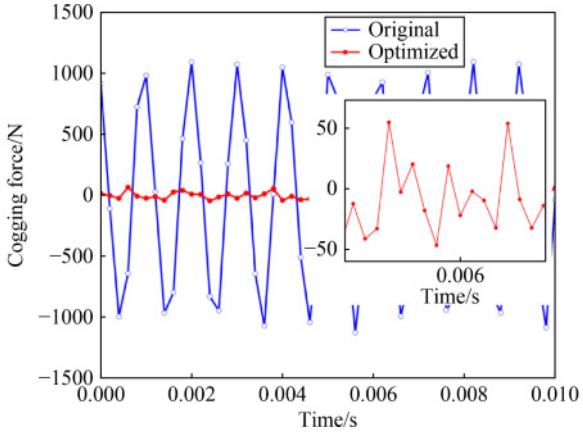

Fig. 10 Cogging force of tubular machine before and after optimization.

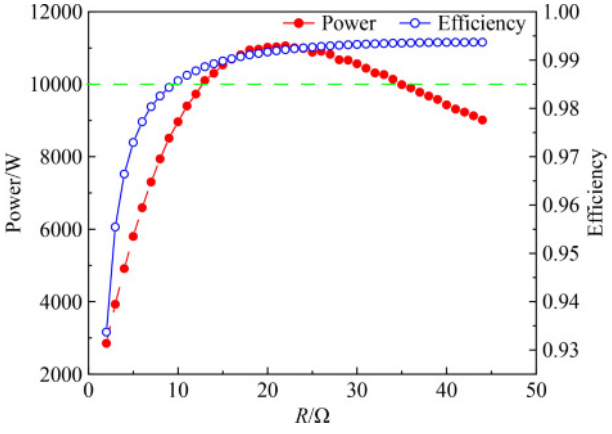

Fig. 11 Output power and efficiency with various external resistance loads.

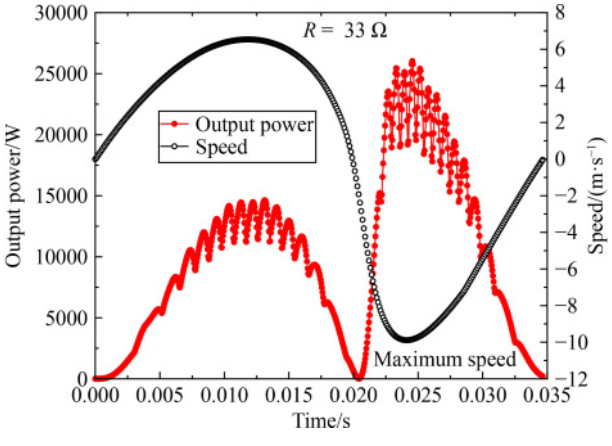

Fig. 12 Output power based on the speed profile in Fig. 7 when $R = 33\ \Omega$.

3.6 Finalize the FPEG dynamic model

The FEM model provides additional insights into the dynamic behavior of the LPMSM and aids in the revision of the corresponding parameters in the dynamic model of the LPMSM, as shown in Section 3.5.2. With this update,

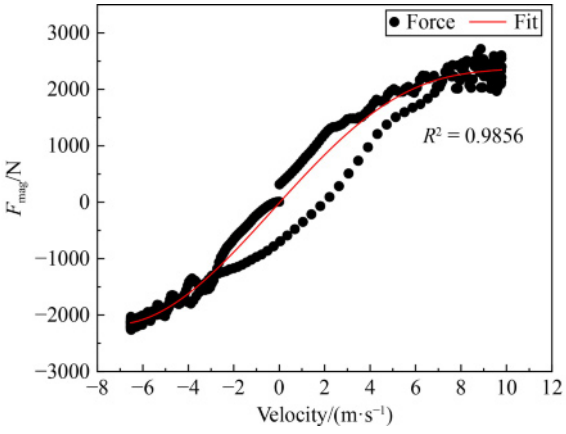

Fig. 13 Simulated piston speed and electromagnetic force in the FEM and the corresponding fitting equation.

the other parameters of the FPEG model may also require adjustments to ensure the stable operation of the model system, which is described in this Section.

Figure 14 shows the piston displacement in the starting and generating states of the FPEG. In the starting state, the piston reached the prescribed BDC point after four cycles. In the generating state, if the electromagnetic force is updated as in Eq. (12), the FPEG operates at a stroke of over 90 mm when the fuel mass per cycle is 22.31 mg, as shown in Fig. 14. This is because of the accurately predicted electromagnetic force and higher generator efficiency of the LPMSM in the dynamic model after the update from the FEM model results. After calibration, a stable FPEG operation at a 90 mm stroke and 30 Hz operational frequency can be achieved when the fuel mass is reduced to 20.06 mg and the spring elasticity coefficient k is set to 6.9×10^4 N/m. The identification of this fuel injection amount and elasticity coefficient finalizes the design of the FPEG system in this study.

The piston trajectory in Fig. 14 demonstrates the stable operation of the optimized FPEG design in MATLAB/Simulink. Figure 15 compares the electric output power produced by the dynamic model and FEM model with a resistance load of 33 Ω. The FEM model indicates that the maximum electric power in the compression and expansion strokes should be 13.9 kW and 23 kW, respectively. The output power profile of the dynamic model has similarities with the FEM model, indicating that the former captured the essential dynamic behavior of the designed LPMSM. Overall, the modeled FPEG had an average electric power of 10.2 kW with a system efficiency of 38.5%.

4 Conclusions

This paper presents the modeling design of a single-piston FPEG through a parameter-decoupling approach.

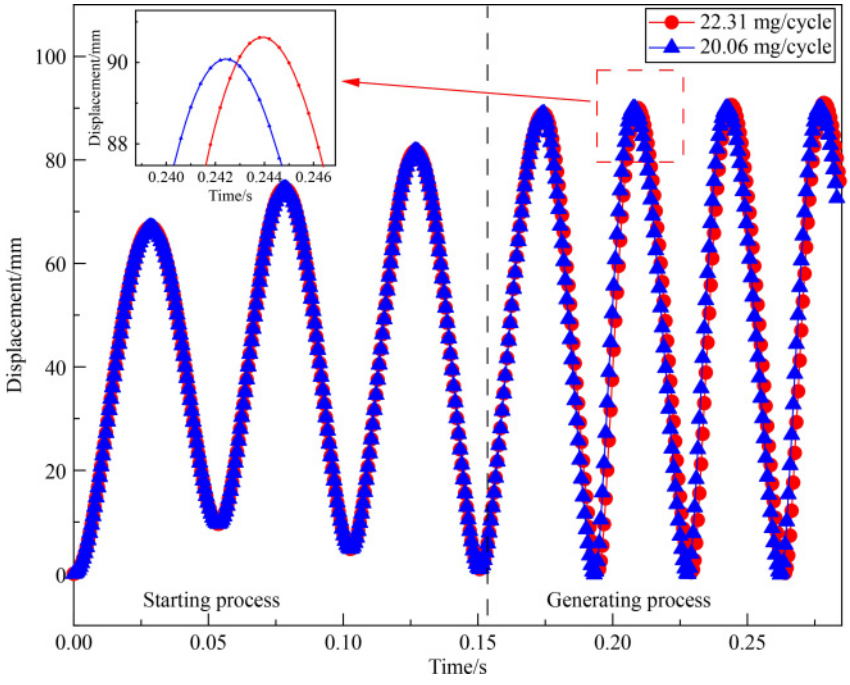

Fig. 14 Displacement of piston in FPEG under two simulated scenarios.

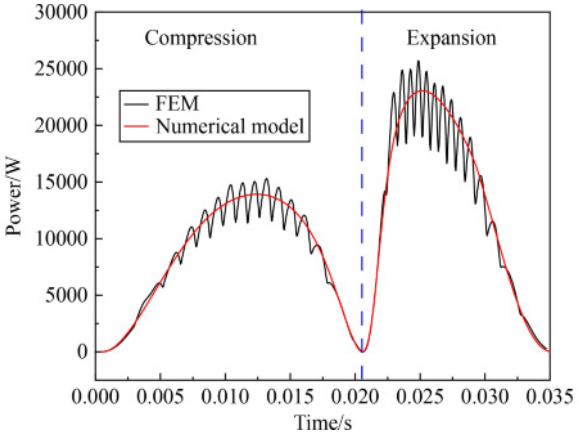

Fig. 15 Comparison of output power produced by the dynamic model and FEM.

Based on the performance target and energy flow analysis, the parameter-decoupling design can determine the key structural and operational parameters of each component in the FPEG, namely a two-stroke engine, an integrated scavenging pump, and LPMSM. According to this data, a dynamic model of the FPEG was developed in MATLAB/Simulink. A detailed FEM model, optimized by the MOGA, was also developed to represent the dynamic behavior of the LPMSM with increased fidelity. The corresponding results from the FEM model were then fed back into the dynamic model to capture a more accurate working performance of the designed LPMSM.

In the dynamic model of the final design of the FPEG system, the piston reached the desired TDC after four cycles in the starting state; and generated 10.2 kW of electric power with a 38.5% system efficiency in the generating state. In addition, the output power profile obtained by the dynamic model has similarities with the FEM model, which proves that the former model captured the essential dynamics of the LPMSM. The final dynamic model establishes a solid foundation for prototype manufacturing and the development of the related FPEG system control.

A prototype of the designed FPEG is currently under construction. A comparison with existing literature will be presented in the future to demonstrate the validity of the developed model.

Acknowledgments This project was supported by the Shanghai Science and Technology Commission (No. 19511108500). We would also like to thank the sponsors of this study.

Competing interests Zhen HUANG is the Editor-in-chief of *Frontiers in Energy*, who was excluded from the peer-review process and all editorial decisions related to the acceptance and publication of this article. Peer-review was handled independently by the other editors to minimise bias.

Notations

FPEG	Free-piston engine generators
LPMSM	Linear permanent magnet synchronous machine
BDC	Bottom dead center
CR	Compression ratio
TDC	Top dead center
D	Bore of engine
D_{sca}	Bore of scavenging pump

F_s	Stoichiometric fuel-air ratio
F_{mag}	Electromagnetic force of LPMSM
H_u	Calorific value of fuel
k	Elasticity coefficient
k_L	Generating load coefficient
m_{fuel}	Injected mass of fuel per cycle
$\dot{m}_f$	Mass flow rate of fuel
$\dot{m}_a$	Mass flow rate of air
n_{crank}	Equivalent crankshaft rotating speed
N_{stroke}	Number of strokes per cycles
P_e	Electrical power
P_{fuel}	Fuel power
Q_{fuel}	Energy from fuel in per cycle
S	Stroke
v_p	Mean speed of piston
x	Displacement of translator from zero point
x_0	Neutral position with a zero spring force
γ	Specific heat ratio
η_c	Fuel conversion efficiency
η_s	System efficiency
δ	Equivalence ratio
ρ_0	Density
λ_v	Volumetric coefficient
λ_p	Pressure coefficient
λ_T	Temperature coefficient
λ_l	Leakage coefficient
λ_T	Temperature coefficient
λ_l	Leakage coefficient

References

1. Ritchie H. Sector by sector: where do global greenhouse gas emissions come from? 2020–9–18, available at website of our world in data
2. Habib S, Khan M M, Abbas F, et al. A framework for stochastic estimation of electric vehicle charging behavior for risk assessment of distribution networks. Frontiers in Energy, 2020, 14(2): 298–317
3. Huang Z, Zhu L, Li A, et al. Renewable synthetic fuel: turning carbon dioxide back into fuel. Frontiers in Energy, 2022, 16(2): 145–149
4. Bahrampour H, Beheshti Marnani A K, Askari M B, et al. Evaluation of renewable energies production potential in the Middle East: confronting the world's energy crisis. Frontiers in Energy, 2020, 14(1): 42–56
5. Zhou Y, Sofianopoulos A, Gainey B, et al. A system-level numerical study of a homogeneous charge compression ignition spring-assisted free piston linear alternator with various piston motion profiles. Applied Energy, 2019, 239: 820–835
6. Haag J, Kock F, Chiodi M, et al. Development approach for the investigation of homogeneous charge compression ignition in a free-piston engine. SAE Technical Pape: 2013–24–0047, 2013
7. Johnson T A, Leick M T, Moses R W. Experimental evaluation of a prototype free piston engine-linear alternator (FPLA) system. SAE Technical Paper: 2016–01–0677, 2016
8. Zhang C, Sun Z X. Trajectory-based combustion control for renewable fuels in free piston engines. Applied Energy, 2017, 187: 72–83
9. Shoukry E, Taylor S, Clark N, et al. Numerical simulation for parametric study of a two-stroke direct injection linear engine. SAE Technical Paper: 2002–01–1739, 2002
10. Fredriksson J, Denbratt I. Simulation of a two-stroke free piston engine. SAE Technical Paper: 2004–01–1871, 2004
11. Mikalsen R, Roskilly A P. The design and simulation of a two-stroke free-piston compression ignition engine for electrical power generation. Applied Thermal Engineering, 2008, 28(5–6): 589–600
12. Mikalsen R, Roskilly A P. The control of a free-piston engine generator. Part 1: fundamental analyses. Applied Energy, 2010, 87(4): 1273–1280
13. Mikalsen R, Roskilly A P. The control of a free-piston engine generator. Part 2: engine dynamics and piston motion control. Applied Energy, 2010, 87(4): 1281–1287
14. Li Q, Xiao J, Huang Z. Simulation of a two-stroke free-piston engine for electrical power generation. Energy & Fuels, 2008, 22(5): 3443–3449
15. Mao J, Zuo Z, Feng H. Parameters coupling designation of diesel free-piston linear alternator. Applied Energy, 2011, 88(12): 4577–4589
16. Jia B, Zuo Z, Tian G, et al. Development and validation of a free-piston engine generator numerical model. Energy Conversion and Management, 2015, 91: 333–341
17. Li K, Zhang C, Sun Z. Precise piston trajectory control for a free piston engine. Control Engineering Practice, 2015, 34: 30–38
18. Zhang C, Sun Z. Using variable piston trajectory to reduce engine-out emissions. Applied Energy, 2016, 170: 403–414
19. Kosaka H, Akita T, Moriya K, et al. Development of free piston engine linear generator system part 1—investigation of fundamental characteristics. SAE Technical Paper: 2014–01–1203, 2014
20. Goto S, Moriya K, Kosaka H, et al. Development of free piston engine linear generator system part 2—investigation of control system for generator. SAE Technical Paper: 2014–01–1193, 2014
21. Moriya K, Goto S, Akita T, et al. Development of free piston engine linear generator system part 3—novel control method of linear generator for to improve efficiency and stability. SAE Technical Paper: 2016–01–0685, 2016
22. Kosaka H, Akita T, Goto S, et al. Development of free piston engine linear generator system and a resonant pendulum type control method. International Journal of Engine Research, 2021, 22(7): 2254–2266
23. Zhu C. Research on single-piston free piston linear generator system. Dissertation for the Master's Degree. Shanghai: Shanghai Jiao Tong University, 2019 (in Chinese)
24. Sun P, Zhang C, Chen J, et al. Decoupling design and verification of a free-piston linear generator. Energies, 2016, 9(12): 1067

25. Chiang C J, Yang J L, Lan S Y, et al. Dynamic modeling of a SI/HCCI free-piston engine generator with electric mechanical valves. Applied Energy, 2013, 102: 336–346
26. Kock F, Haag J, Friedrich H E. The free piston linear generator—development of an innovative, compact, highly efficient range-extender module. SAE Technical Paper: 2013–01–1727, 2013,
27. Kock F, Heron A, Rinderknecht F, et al. The free-piston linear generator potentials and challenges. MTZ Worldwide, 2013, 74(10): 38–43
28. Yamanaka Y, Nirei M, Sato M, et al. Design of linear synchronous generator suitable for free-piston engine linear generator system. In: Proceeding of 2017 11th International Symposium on Linear Drives for Industry Applications (LDIA), Osaka: Japan, 2017
29. Mattarelli E, Rinaldini C A, Savioli T. Port design criteria for 2-stroke loop scavenged engines. SAE Technical Paper: 2016–01–0610, 2016,
30. Bloch H B, Hoefner J J. Reciprocating Compressors: Operation and Maintenance. Woburn: Butterworth-Heinemann, 1996
31. Hanlon P. Compressor Handbook. New York: McGraw-Hill, 2001
32. Shi T. Research on integrated scavenging and optimization of free piston linear generator. Dissertation for the Master's Degree. Shanghai: Shanghai Jiao Tong University, 2020 (in Chinese)
33. Atkinson C M, Petreanu S, Clark N N, et al. Numerical simulation of a two-stroke linear engine-alternator combination. SAE Technical Paper: 1999-01-0921, 1999
34. Johnson D L. Miniature free-piston engine compressor. Dissertation for the Master's Degree. Minneapolis: University of Minnesota, 2015
35. Feng H, Song Y, Zuo Z, et al. Stable operation and electricity generating characteristics of a single-cylinder free piston engine linear generator: Simulation and experiments. Energies, 2015, 8(2): 765–785
36. Boldea I. Linear Electric Machines, Drives, and MAGLEVs Handbook. Boca Raton: CRC Press, 2013